Mechanistic Studies of the Formation of Zirconium Alkylidene Complexes [η^5-C_5H_3-1,3-($SiMe_2CH_2PPr^i_2$)$_2$]Zr=CHR(Cl) (R = Ph, $SiMe_3$)

Michael D. Fryzuk,*,† Paul B. Duval,† Shane S. S. H. Mao,† Michael J. Zaworotko,‡ and Leonard R. MacGillivray‡

Contribution from the Department of Chemistry, University of British Columbia, 2036 Main Mall, Vancouver, B.C., Canada V6T 1Z1, and Department of Chemistry, St. Mary's University, Halifax, N.S., Canada B3H 3C3

Received August 18, 1998

Abstract: The reaction of $[P_2Cp]ZrCl_3$ (**1**) with 2 equiv of KCH_2Ph generates an equilibrium mixture of alkyl complexes consisting of $[P_2Cp]ZrCl_2(CH_2Ph)$ (**2**), $[P_2Cp]ZrCl(CH_2Ph)_2$ (**3**), and $[P_2Cp]Zr(CH_2Ph)_3$ (**4**). Thermolysis of this mixture yields the alkylidene complex $[P_2Cp]Zr{=}CHPh(Cl)$ (**5**) in 85% overall yield. Kinetic studies reveal a composite mechanism that incorporates the above preequilibrium, followed by an intramolecular α-abstraction reaction of dibenzyl **3** which follows a first-order rate, with the rate parameters $\Delta H^{\ddagger} = 19(1)$ kcal mol^{-1} and $\Delta S^{\ddagger} = -22(5)$ cal^{-1} mol K^{-1}. A kinetic isotope effect of 3.0(5) was measured at 70 °C for the perdeuterated analogue $[P_2Cp]ZrCl(CD_2C_6D_5)_2$. The reaction of **1** with 2 equiv of $LiCH_2EMe_3$ (E = C, Si) produces a similar equilibrium mixture as observed for the benzyl analogues, consisting of $[P_2Cp]ZrCl_2(CH_2EMe_3)$ (**7**), $[P_2Cp]Zr(CH_2EMe_3)_3$ (**8**), and $[P_2Cp]ZrCl(CH_2EMe_3)_2$ (**9**). Thermolysis of this mixture yields $[P_2Cp]Zr{=}CHEMe_3(Cl)$ (**6**). A kinetic analysis conducted on **9** (E = Si) indicated a first-order reaction from which the activation parameters $\Delta H^{\ddagger} = 6(1)$ kcal mol^{-1} and $\Delta S^{\ddagger} = -62(5)$ cal mol^{-1} K^{-1} were obtained. The results indicate that reaction rates follow the order $CH_2Ph > CH_2SiMe_3 > CH_2CMe_3$, an exact reversal of the trend for the homoleptic Ta systems $Ta(CH_2R)_5$. The role of phosphine coordination is discussed to account for this trend. A crystal structure determination obtained for **6b** reveals an α-agostic interaction and a structure analogous to that of **5**.

Introduction

Metal alkylidene[1] complexes continue to generate interest as intermediates in a number of important catalytic reactions involving olefins, including alkene metathesis[2,3] and related transformations such as ring-opening metathesis polymerization (ROMP)[4−7] and ring-closing metathesis (RCM)[8,9] catalysis. Many examples of alkylidene complexes are known for the groups 5 and 6 metals,[10−12] which is in stark contrast to the paucity of group 4 derivatives.[13,14] The reason for the discrepancy between the above-mentioned groups has been attributed to the mechanism by which these complexes are formed; as shown in Scheme 1, a sterically congested polyalkyl precursor is necessary since this promotes α-abstraction between two cis-disposed alkyl ligands.[1]

Scheme 1

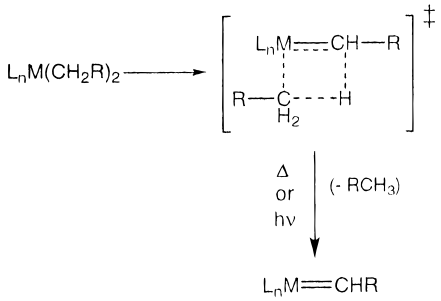

For groups 5 and 6 precursors this arrangement can be met either with bulky homoleptic alkyl complexes such as $Ta(CH_2CMe_3)_5$[15] or similar derivatives such as $Cp^*TaCl_2(CH_2CMe_3)_2$.[16] However, the analogous group 4 complexes contain at least one less alkyl ligand and hence are at a considerable disadvantage to achieve a similarly crowded coordination sphere. Therefore,

† University of British Columbia.
‡ St. Mary's University.

(1) *Comprehensive Organometallic Chemistry*, 2nd ed.; Wilkinson, G., Stone, F. G. A., Abel, E. W., Eds.; Pergamon: New York, 1995; Vol. 3.
(2) Schuster, M.; Blechert, S. *Angew. Chem., Int. Ed. Engl.* **1997**, *36*, 2036.
(3) Irvin, K. J.; Mol, J. C. *Olefin Metathesis and Metathesis Polymerization*; Academic Press: New York, 1997.
(4) Gilliom, L. R.; Grubbs, R. H. *J. Am. Chem. Soc.* **1986**, *108*, 733.
(5) Schrock, R. R. *Acc. Chem. Res.* **1990**, *23*, 158.
(6) Bazan, G. C.; Oskam, J. H.; Cho, H.-N.; Park, L. Y.; Schrock, R. R. *J. Am. Chem. Soc.* **1991**, *113*, 6899.
(7) Conticello, V. P.; Gin, D. L.; Grubbs, R. H. *J. Am. Chem. Soc.* **1992**, *114*, 9708.
(8) Pernerstorfer, J.; Schuster, M.; Blechert, S. *J. Chem. Soc., Chem. Commun.* **1997**, 1949.
(9) Grubbs, R. H.; Miller, S. J.; Fu, G. C. *Acc. Chem. Res.* **1997**, *28*, 4446.
(10) Schrock, R. R. *Acc. Chem. Res.* **1979**, *12*, 98.
(11) Wallace, K. C.; Liu, A. H.; Dewan, J. C.; Schrock, R. R. *J. Am. Chem. Soc.* **1988**, *110*, 4964.
(12) Feldman, J.; Schrock, R. R. *Prog. Inorg. Chem.* **1991**, *39*, 1.
(13) Wengrovius, J. H.; Schrock, R. R. *J. Organomet. Chem.* **1981**, *205*, 319.
(14) Beckhaus, R. *Angew. Chem., Int. Ed. Engl.* **1997**, *36*, 686.
(15) Schrock, R. R. *J. Am. Chem. Soc.* **1974**, *96*, 6796.
(16) Wood, C. D.; McLain, S. J.; Schrock, R. R. *J. Am. Chem. Soc.* **1979**, *101*, 3210.

10.1021/ja982969h CCC: $18.00
Published on Web 03/03/1999

most group 4 alkylidene complexes reported thus far have required the addition of either inter- or intramolecular phosphine donors,[17,18] and of these examples, only a few Ti derivatives have been isolated as thermally stable compounds.[19−23]

We are currently exploring the organometallic chemistry of early transition-metals and f-block elements stabilized by the tridentate ligand [η^5-C_5H_3-1,3-($SiMe_2CH_2PPr^i_2$)$_2$] ([P_2Cp]). This system has allowed for the isolation and solid-state structure determination of the first stable zirconium alkylidene complex [P_2Cp]Zr=CHPh(Cl) (**5**).[24] The high yield and overall stoichiometry of this product suggested that the reaction proceeds via a thermally induced α-abstraction of the dialkyl precursor [P_2Cp]Zr$Cl(CH_2Ph)_2$ (**3**). However, this species was not initially detected and therefore was assumed to be an unobserved intermediate in this reaction.[24] Further investigation has now provided for the detection of **3** and permitted us to study the mechanism of its transformation to **5**. Although the mechanistic

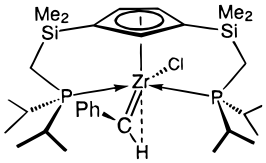

5

details of alkylidene formation have received considerable attention,[25] the kinetic study presented here provides the first insight into this reaction from the perspective of group 4 derivatives.

The generality of this reaction has been extended to the synthesis of the alkylidene analogues, [P_2Cp]Zr=CHEMe_3(Cl) (**6a:** E = C, **6b:** E = Si). A kinetic study of the formation of **6b** is included in this report as a comparison to the mechanism determined for **5**, along with the crystal structure determination for **6b**.

Results and Discussion

NMR Spectroscopic Identification of [P_2Cp]Zr$Cl(CH_2Ph)_2$ (3). The starting complex [P_2Cp]$ZrCl_3$ (**1**) reacts rapidly with 1 equiv of KCH_2Ph in THF to produce the monobenzyl complex [P_2Cp]$ZrCl_2(CH_2Ph)$ (**2**), which can be isolated with difficulty as red crystals from a cold (−40 °C), concentrated, hexamethyldisiloxane solution. Similarly, **1** reacts readily with 3 equiv of KCH_2Ph in THF to generate cleanly the tribenzyl derivative [P_2Cp]Zr$(CH_2Ph)_3$ (**4**) as a hydrocarbon-soluble orange oil. The solution behavior of these species as monitored by variable-temperature NMR spectroscopy has been described previously.[26] At ambient temperature the pendant phosphines of **2** are fluxional, undergoing rapid exchange via an associative pathway. In the slow limit of this process, one phosphine coordinates to the metal while the other is dissociated. By comparison, in **4** the three bulky benzyl ligands crowd the metal center and prevent either phosphine from coordinating, leaving both sidearms dangling at all temperatures.

In contrast to these results, treating the starting trichloride complex **1** with 2 equiv of KCH_2Ph in THF does not give the dibenzyl complex [P_2Cp]Zr$Cl(CH_2Ph)_2$ (**3**) as the sole product, but instead yields a thermally and photochemically labile compound isolated as a greenish-orange oil consisting of a mixture of **2**, **3**, and **4**, in the ratio of 5:4:5, respectively, at room temperature (eq 1):

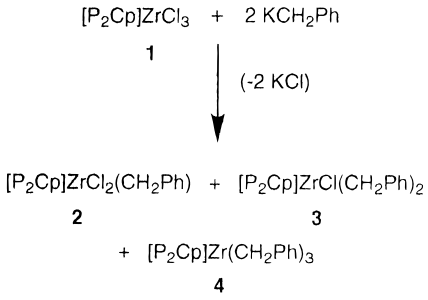

(1)

2, **3** and **4** are all observed together as products of this reaction as long as the stoichiometry of KCH_2Ph used is greater than 1 equiv and less than 3 equiv, the relative proportion of tribenzyl **4** present in the mixture increasing with the amount of benzyl reagent used. Attempts to separate individual species from this mixture have repeatedly proved unsuccessful. The subsequent thermal or photochemical reaction of this ensemble to produce the benzylidene complex [P_2Cp]Zr=CHPh(Cl) (**5**) will be discussed later.

The identification of **3** within this mixture was nontrivial and is based on the assignment of resonances in the ^{1}H and ^{31}P{^{1}H} NMR spectra by comparison to those resonances attributed to known **2** and **4**. The coexistence of all three species in solution generates a complicated ^{1}H NMR spectrum with some peaks overlapping even at 500 MHz, thereby rendering some resonances unassignable. However, the integration of those resonances attributable to **3** supports the stoichiometry of the compound as a dibenzyl complex (two CH_2Ph ligands per [P_2Cp] moiety).

The ambient temperature ^{31}P{^{1}H} NMR spectrum of the reaction mixture reveals a broad singlet for **3** at 0.5 ppm, which sharpens as the temperature is elevated to 95 °C. As the temperature is lowered below room temperature, this peak gradually broadens until it disappears into the baseline near −70 °C, beyond which a reappearance of new peaks is not observed even down to −95 °C. These observations are consistent with fluxional coordination of the sidearm phosphines to the metal center, as previously noted with other [P_2Cp]ZrR_xCl_{3-x} complexes.[26]

The resonances due to the benzylic (CH_2Ph) protons of **3** are temperature dependent, a feature that is not observed in the corresponding spectra of either **2** or **4**. This portion of the ^{1}H NMR spectrum of the mixture is relatively unobscured, which permitted a variable-temperature study. At −40 °C the benzylic protons of **3** give rise to a doublet of multiplets centered near 2.45 ppm; the pattern resembles an AB multiplet with additional coupling to phosphorus-31. As the temperature is raised to −10 °C this doublet of multiplets evolves into a doublet of doublets, which gradually converges to two broad singlets at 30 °C. Eventually these peaks coalesce as the temperature approaches 40 °C, and a further temperature increase gradually sharpens

(17) Schwartz, J.; Gell, K. I. *J. Organomet. Chem.* **1980**, *184*, C1.
(18) Hartner, F. W.; Schwartz, J.; Clift, S. M. *J. Am. Chem. Soc.* **1983**, *105*, 640.
(19) van der Heijden, H.; Hessen, B. *J. Chem. Soc., Chem. Commun.* **1995**, 145.
(20) van Doorn, J. A.; van der Heijden, H.; Orpen, A. G. *Organometallics* **1995**, *14*, 1278.
(21) Binger, P.; Muller, P.; Benn, R.; Mynott, R. *Angew. Chem., Int. Ed. Engl.* **1989**, *28*, 610.
(22) Sinnema, P.-J.; Veen, L.; Spek, A. L.; Veldman, N.; Teuben, J. H. *Organometallics* **1997**, *16*, 4245.
(23) Kahlert, S.; Görls, H.; Scholz, J. *Angew. Chem., Int. Ed. Engl.* **1998**, *37*, 1857.
(24) Fryzuk, M. D.; Mao, S. S. H.; Zaworotko, M. J.; MacGillivray, L. R. *J. Am. Chem. Soc.* **1993**, *115*, 5336.
(25) Li, L.; Hung, M.; Xue, Z. *J. Am. Chem. Soc.* **1995**, *117*, 12746.
(26) Fryzuk, M. D.; Mao, S. S. H.; Duval, P. B.; Rettig, S. J. *Polyhedron* **1995**, *14*, 11.

Table 1. Equilibrium Concentrations of **2**, **3**, and **4** from Mixed Solutions at 25 °C and the Resulting Equilibrium Constant (*K*) Calculated According to Eq 2

[**2**] (M)	[**3**] (M)	[**4**] (M)	*K*
0.55	0.12	0.04	0.7
0.23	0.10	0.07	0.5
0.15	0.11	0.17	0.7
0.04	0.07	0.17	0.7

this singlet further. To account for these observations, in the low-temperature limit, it is proposed that the benzyl ligands of **3** are chemically equivalent but the methylene protons are inequivalent; a structure based on a pseudo trigonal bipyramid with one phosphine arm coordinated and the other dangling is shown below. As the temperature is raised the rate of phosphine donor exchange gradually increases until it coincides with the NMR time scale at coalescence, and eventually in the fast exchange limit of this process a singlet is observed as an average of two chemical environments. Thus on average, two equivalent benzyl groups are present and only one pendant phosphine donor is coordinated.

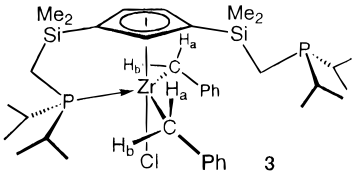

3

Equilibrium between $[P_2Cp]ZrCl_2(CH_2Ph)$ (2), $[P_2Cp]ZrCl(CH_2Ph)_2$ (3), and $[P_2Cp]Zr(CH_2Ph)_3$ (4). Monobenzyl **2** and tribenzyl **4** are each isolable in high yield from reactions conducted under the appropriate stoichiometric conditions, yet as already mentioned, attempts to prepare dibenzyl **3** always result in mixtures. A possible explanation for the coexistence of **2**, **3**, and **4** from the reaction in eq 1 is that there is an equilibrium between dibenzyl **3**, monobenzyl **2**, and tribenzyl **4** (eq 2):

$$\underset{\mathbf{2}}{[P_2Cp]ZrCl_2(CH_2Ph)} + \underset{\mathbf{4}}{[P_2Cp]Zr(CH_2Ph)_3} \underset{}{\overset{K}{\rightleftharpoons}} \underset{\mathbf{3}}{2\ [P_2Cp]ZrCl(CH_2Ph)_2} \qquad (2)$$

In support of this proposal, when pure **2** and **4** are mixed in solution, one immediately observes the formation of **3**, irrespective of the order of addition, and ultimately a mixture of all three compounds. The ratio of species observed in the final reaction mixture depends on the relative amounts of monobenzyl **2** and tribenzyl **4** initially added. Table 1 shows the equilibrium concentrations obtained from separately prepared solutions in which the initial proportions of **2** and **4** added together were varied. From the data, it is evident that these species are indeed in equilibrium (eq 2) with an equilibrium constant ($K = [\mathbf{3}]^2/[\mathbf{2}][\mathbf{4}]$) equal to 0.7(1) at 25 °C. The estimated uncertainty in *K* is a function of the imprecision in the integration measurements of the ^{1}H NMR spectra, as evaluated from repetitive experiments.

Variable-temperature NMR experiments were then conducted on sample mixtures of **2**, **3**, and **4** to obtain thermodynamic information from the temperature dependence of the equilibrium constant depicted in eq 2. Because of the aforementioned fluxional behavior of various species and by the temperature dependence of the chemical shifts of some resonances, precise integration measurements of the spectra obtained proved difficult. As a result, the van't Hoff plots obtained were subject to considerable uncertainty in the linear fits, and reproducible values for the thermodynamic parameters $\Delta H°$, $\Delta S°$, and $\Delta G°$ could not be calculated. However, the measurements were sufficiently reliable to be able to discern a small increase in the concentration of **3** relative to **2** and **4** as the temperature was increased over a wide (−65 to 60 °C) range. Therefore, a qualitative assessment of the thermodynamics in this reaction could be made. The minimal temperature dependence of the equilibrium constant apparent from the results suggests that the magnitude of $\Delta H°$ is fairly small, a positive value being inferred from the observed increase in *K* with temperature. Also, as there are an equal number of species on each side of eq 2 and all are approximately similar in structure, one could argue that $\Delta S°$ should also be relatively small. Overall, this would give a low value for $\Delta G°$ in this reaction, although admittedly there is considerable uncertainty associated with the assumptions made in this analysis.

Scheme 2

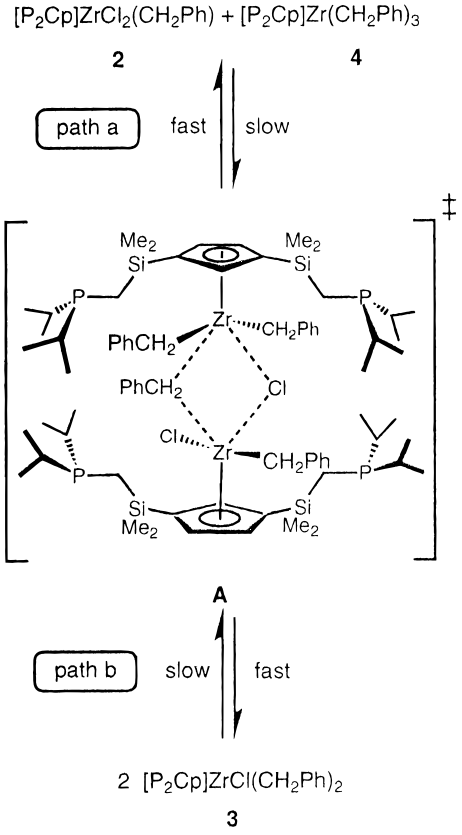

The mechanism that converts monobenzyl **2** and tribenzyl **4** to 2 equiv of dibenzyl **3** involves a mutual exchange of benzyl and chloro ligands. An intermediate is not observed in this reaction, but a plausible candidate could be the dinuclear adduct **A** shown in Scheme 2. There are two options for dissociation of the bridging ligands in complex **A**: path a regenerates **2** and **4**, while path b leads to the formation of 2 equiv of **3**; both pathways are consistent with the reaction in eq 2.

It should be stated at this point that both mononuclear **3** and the dinuclear adduct **A** possess an identical stoichiometry of two benzyl ligands for each $[P_2Cp]$ group. The identification of the species observed in equilibrium with monobenzyl **2** and tribenzyl **3** as mononuclear **3** was ascertained from the equi-

Scheme 3

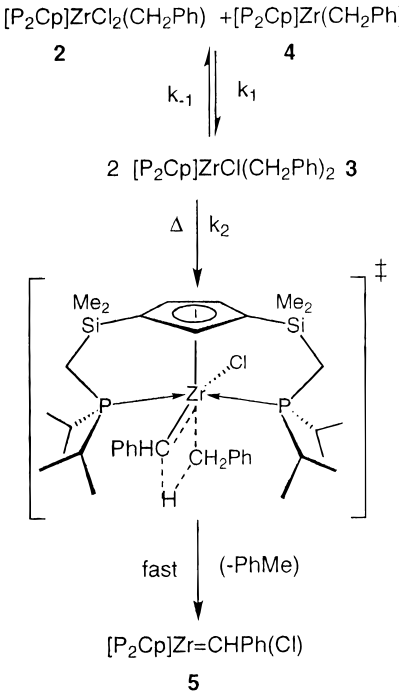

librium concentration measurements. As shown in Table 1, a process involving dinuclear **A** in direct equilibrium with monobenzyl **2** and tribenzyl **4** (i.e., in which path b in Scheme 2 is omitted) is not in accord with the data. An equilibrium constant calculated assuming a dinuclear complex would require that $K = [\mathbf{A}]/[\mathbf{2}][\mathbf{4}]$; this in turn requires that the values for [**A**] determined by integration of the NMR spectra would equal one-half the values listed for **3** in Table 1, and therefore shows poor correlation between the separate sample mixtures. Furthermore, if this equilibrium were in effect then dilution of the reaction mixture should induce further disproportionation of **A** to restore the equilibrium, a feature that is not observed.

Mechanistic Studies on the Formation of [P₂Cp]Zr=CHPh(Cl) (5). As previously reported,[24] thermolysis of a toluene solution of the reaction mixture consisting of **2**, **3**, and **4** at 65 °C for 24 h produces the alkylidene complex [P₂Cp]-Zr=CHPh(Cl) (**5**). The same result is obtained when the reaction mixture is exposed to visible light for a period of 12 h. **5** is thermally stable and can be isolated as moderately air- and moisture-sensitive orange crystals from cold pentane in high yield (85%).

The unusual transformation of the mixture of benzyl complexes **2**, **3**, and **4** to produce alkylidene **5** prompted us to investigate the mechanism employed. Since it was found that each of **2** and **4** is thermally and photochemically stable under the conditions that generate alkylidene **5** from the mixture, it seemed likely that the dibenzyl complex **3** is the precursor to the alkylidene **5** via α-abstraction; this is summarized in Scheme 3. Accordingly, the continued depletion of **3** in forming **5** would perturb the preequilibrium in Scheme 3, thus prompting the conversion of additional monobenzyl **2** and tribenzyl **4** to replenish **3**, eventually resulting in the observed high yield production of **5**. Added support that **3** is the reactive species is provided by heating reaction mixtures consisting of unequal proportions of **2** and **4**. In each case the formation of **5** ceases when the precursor **3** can no longer be replenished, which occurs once the limiting component (either **2** or **4**) as a source for **3** has been consumed.

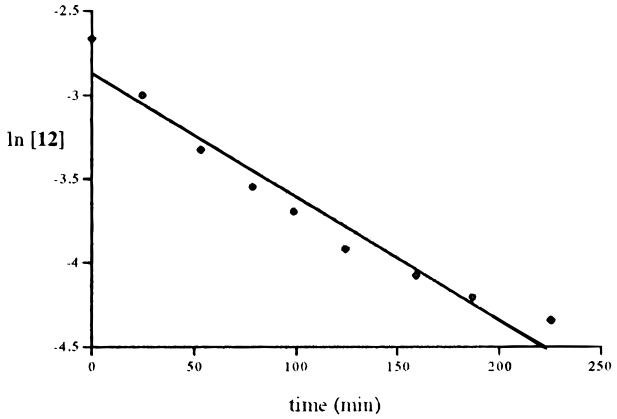

Figure 1. Nonlinear fit to the first-order decomposition of **3** (at 353 K).

Table 2. Estimated Rate Constants for the First-Order α-Abstraction of **3**

T (K)	$10^4 k_2$ (s^{-1})
343(1)	0.7(2)
353(1)	1.6(2)
358(1)	2.5(2)
368(1)	5.4(3)

A kinetic analysis of the thermolysis of this reaction mixture was conducted by monitoring the $^{31}P\{^1H\}$ NMR spectra for separate reactions performed at 70, 80, 85, and 95 °C, respectively. A similar study was also conducted at 70 °C on the perdeuterated analogue $[P_2Cp]ZrCl(CD_2C_6D_5)_2$ (**3-d₇**) to examine a possible kinetic isotope effect. In all instances the decline in [**3**] followed a pattern as shown in Figure 1. The nonlinear fit of the plot of ln[**3**] versus time illustrates a departure from first-order kinetics; the preequilibrium in this composite mechanism is likely responsible for these complicated results. The steep initial decrease in the concentration of **3** corresponds more closely to the actual first-order α-abstraction reaction rate, but curvature in the plot in Figure 1 arises due to a steady decrease in the observed rate (k_{obs}) as the continued lowering in the concentrations of the equilibrium species makes it more difficult to replenish **3** from bimolecular collisions of **2** and **4**.

To evaluate the complicating factor of the preequilibrium, the results were simulated (Chemical Kinetics Simulator)[27] from input of the initial concentrations and the kinetic parameters k_1, k_{-1}, and k_2. Knowledge of the approximate equilibrium constant K gives the ratio k_1/k_{-1}, with limits for these values set ($1 > k > 10^{-3}$ s^{-1}) by the lack of exchange broadening observed in the line widths of the equilibrium species in the NMR spectra, and by the observation of k_2 as the slow step in this composite reaction mechanism. A more precise estimate of these parameters, as well as the rate constant k_2 for the irreversible α-abstraction step, could be made by iteration of the simulation results to give the best agreement with the experimentally determined changes in [**3**], [**4**], and [**5**] as a function of time; only a very narrow range of values of k_2 (given in Table 2) produces the observed values of [**3**], [**4**], and [**5**] for a given temperature. The inclusion of the preequilibrium in the simulation analysis reproduces the characteristic decay of dibenzyl **3** depicted in Figure 1.

The rate constants (k_2) obtained for each temperature from the simulated data are shown in Table 2; a kinetic isotope effect of 3.0(0.5) was observed at 70 °C for the perdeuterated species, in support of rate-determining C−H bond activation[16,25] in a concerted, four-centered transition state as shown in Scheme

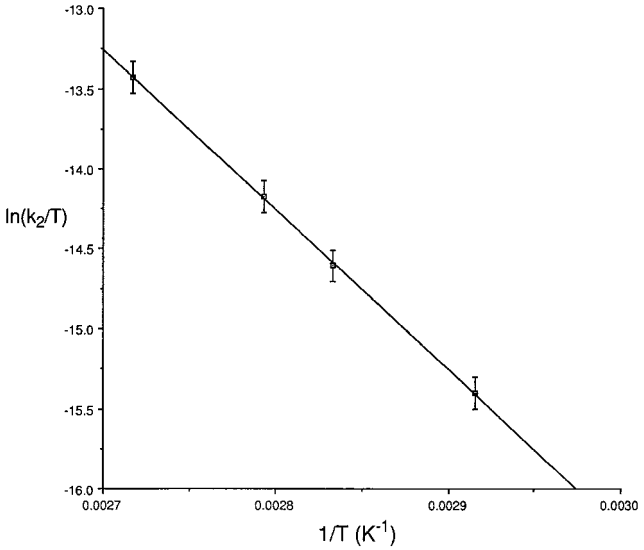

Figure 2. Eyring plot of the first-order decomposition of **3** (arbitrary error bars of ±0.1 are indicated).

3. From the Eyring plot in Figure 2 the activation parameters $\Delta H^{\ddagger} = 19(1)$ kcal mol^{-1} and $\Delta S^{\ddagger} = -22(5)$ cal mol^{-1} K^{-1} were obtained. The value for $\Delta H^{\ddagger}$ is in accord with kinetic studies conducted on other systems involving alkylidene formation and related C−H activation processes.[28−30] In those studies $\Delta H^{\ddagger}$ ranges between 20 and 30 kcal mol^{-1}. However, the experimentally determined value of $\Delta S^{\ddagger}$ for **3** is rather large in comparison to these other systems (typically between 0 and −10 cal mol^{-1} K^{-1}), although the decomposition of $Ti(CH_2CMe_3)_4$ via an alkylidene intermediate has a similar large negative $\Delta S^{\ddagger} = -16$ cal mol^{-1} K^{-1}.[31] An in-depth analysis of the kinetic results for **3** will be given in conjunction with the analogous results for the α-abstraction of $[P_2Cp]ZrCl(CH_2SiMe_3)_2$ (**9b**) to give alkylidene $[P_2Cp]Zr{=}CHSiMe_3(Cl)$ (**6b**).

Other Zirconium Alkylidene Complexes. In view of the success in the synthesis of the benzylidene complex **5**, we were interested in testing both the generality of this reaction mechanism and the versatility of the $[P_2Cp]$ ligand in stabilizing other Zr alkylidene complexes. Two examples of alkyl groups that have been commonly chosen for the synthesis of alkylidene complexes of the early transition-metals are the neopentyl (CH_2CMe_3)[10] and neosilyl (CH_2SiMe_3) ligands.[25] Treatment of **1** with 2 equiv of $LiCH_2EMe_3$ (E = C, Si) in toluene at −78 °C yields a bright yellow oil after workup. Thermolysis of this material in toluene at 95 °C generates the corresponding alkylidene complex $[P_2Cp]Zr{=}CHEMe_3(Cl)$ (**6a:** E = C, **6b:** E = Si) (Scheme 4). The formation of **6a** requires 6 days at 95 °C, while the analogous reaction to produce **6b** is complete within 3 days under the same conditions.

The neopentylidene (**6a**) was obtained as a green oil, contaminated with inseparable side-products (approximately 20% by NMR spectroscopy), presumably a result of the prolonged duration of the thermolysis. Diagnostic of the alkylidene moiety is the singlet observed at 8.56 ppm in the ^{1}H NMR spectrum and the triplet at 209 ppm in the $^{13}C\{^1H\}$ NMR spectrum, for the alkylidene proton ($Zr{=}CHCMe_3$) and carbon, respectively. In contrast, the silyl analogue **6b** can be isolated as thermally stable, air- and moisture-sensitive yellow crystals in very good yield. Spectroscopic data for **6b** reveal a singlet in the ^{1}H NMR spectrum at 8.99 ppm for the alkylidene proton ($Zr{=}CHSiMe_3$) and a triplet at 225 ppm in the $^{13}C\{^1H\}$ NMR spectrum for the alkylidene carbon ($Zr{=}CHSiMe_3$); the triplet pattern in the $^{13}C\{^1H\}$ NMR spectrum arises from $^2J_{PC}$ coupling to two equivalent phosphines.

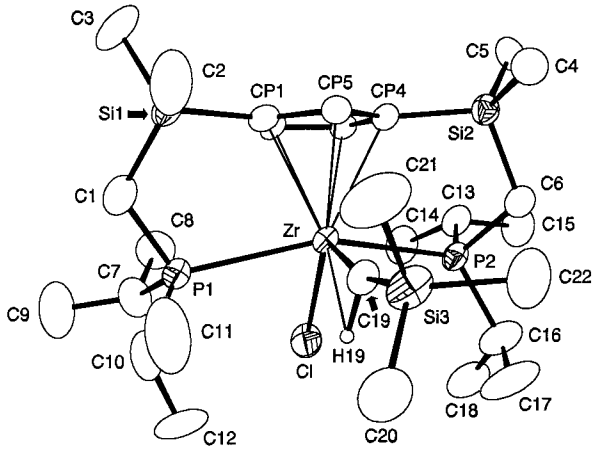

Figure 3. ORTEP view of **6b**; 50% probability thermal ellipsoids are shown for the non-hydrogen atoms and H(19).

Scheme 4

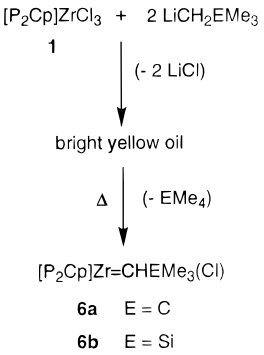

An X-ray structure determination of **6b** was undertaken; the molecular structure is shown in Figure 3, with selected bond lengths and bond angles given in Table 3. The very short Zr−C bond distance of 2.015(9) Å is similar to that of 2.024(4) Å for Zr benzylidene **5**.[24] As also observed for **5**, the alkylidene fragment in **6b** is oriented syn to the unique cyclopentadienyl carbon, with the α-hydrogen atom directed below the metal center to form the same type of agostic C−H interaction. This hydrogen was located and refined, and the Zr···H distance of 2.28(8) Å, together with the distorted Zr−C−Si angle of 164.3(6)°, is characteristic of an α-agostic C−H bond.[32] All other bond lengths and angles are similar to those in the corresponding alkylidene **5**.[24]

To examine the formation of **6a** and **6b** in comparison to the mechanism determined for **5**, reaction mixtures derived according to Scheme 4 were studied by NMR spectroscopy prior to the thermolysis. The spectra obtained exhibit a complexity that has been similarly noted from the products of the analogous reaction in eq 1, suggesting the occurrence of an equilibrium mixture of the corresponding mono-, di-, and trialkyl complexes. To help assign these species, the alkyl complexes $[P_2Cp]$-

(27) Hinsberg, W.; Houle, F., Almaden Research Center, IBM, 1996, San Jose, CA.

(28) Thorn, M. G.; Hill, J. E.; Waratuke, S. A.; Johnson, E. S.; Fanwick, P. E.; Rothwell, I. P. *J. Am. Chem. Soc.* **1997**, *119*, 8630.

(29) Vaughan, W. M.; Abboud, K. A.; Boncella, J. M. *J. Am. Chem. Soc.* **1995**, *117*, 11015.

(30) McDade, C.; Green, J. C.; Bercaw, J. E. *Organometallics* **1982**, *1*, 1629.

(31) Cheon, J.; Rogers, D. M.; Girolami, G. S. *J. Am. Chem. Soc.* **1997**, *119*, 6804.

(32) Brookhart, M.; Green, M. L. H.; Wong, L. L. *Prog. Inorg. Chem.* **1988**, *36*, 1.

Table 3. Selected Bond Lengths (Å) and Bond Angles (deg) for **6b**

Zr(1)−Cl(1)	2.508(3)	Zr(1)−P(1)	2.838(3)
Zr(1)−P(2)	2.820(3)	Zr(1)−CP(1)	2.569(8)
Zr(1)−CP(2)	2.549(8)	Zr(1)−CP(3)	2.528(8)
Zr(1)−CP(4)	2.555(8)	Zr(1)−CP(5)	2.555(8)
Zr(1)−Cent	2.577(8)	Zr(1)−C(19)	2.015(9)
P(1)−Cl(1)	1.827(9)	P(1)−C(7)	1.855(11)
P(1)−C(10)	1.845(12)	P(2)−C(6)	1.810(9)
P(2)−C(13)	1.881(10)	P(2)−C(16)	1.839(11)
Si(1)−CP(1)	1.878(9)	Si(1)−Cl(1)	1.794(11)
Si(1)−CP(4)	1.855(9)	Cp(1)−CP(2)	1.437(12)
Cp(1)−CP(5)	1.398(13)	Cp(2)−CP(3)	1.405(12)
CP(3)−C(4)	1.412(16)	Si(3)−C(19)	1.848(9)
Si(3)−C(20)	1.841(12)	C(19)−H(19)	1.10(8)
Zr(1)−H(19)	2.28(8)		

Cl(1)−Zr(1)−P(1)	76.48(8)	Cl(1)−Zr(1)−P(2)	78.44(9)
Cl(1)−Zr(1)−C(19)	108.0(3)	Zr(1)−C(19)−Si(3)	164.3(6)
P(1)−Zr(1)−P(2)	154.91(8)	Si(3)−C(19)−H(19)	106.5
P(1)−Zr(1)−C(19)	95.9(3)	P(2)−Zr(1)−C(19)	92.5(3)
Zr(1)−P(1)−Cl(1)	111.8(3)	Zr(1)−P(1)−C(7)	116.7(4)
Zr(1)−P(2)−C(6)	111.7(4)	Cp1(1)−Si(1)−C(1)	106.8(4)
Cp(4)−Si(2)−C(4)	110.6(4)	Si(1)−CP(1)−CP(2)	123.2(7)
Si(1)−CP(1)−CP(5)	131.0(7)	P(1)−C(1)−Si(1)	119.1(6)
P(2)−C(6)−Si(2)	113.6(5)	Cl(1)−Zr(1)−Cent	141.23(8)
P(1)−Zr(1)−Cent	100.42	P(2)−Zr(1)−Cent	98.62(7)
C(19)−Zr(1)−Cent	110.7(3)	Zr(1)−C(19)−H(19)	89.5(5)

$ZrCl_2(CH_2EMe_3)$ (**7a:** E = C, **7b:** E = Si) and $[P_2Cp]Zr(CH_2EMe_3)_3$ (**8a:** E = C, **8b:** E = Si) were independently prepared from reactions of **1** with the appropriate stoichiometry of $LiCH_2EMe_3$ in toluene (eq 3, 4):

$$[P_2Cp]ZrCl_3\ (\mathbf{1}) + LiCH_2EMe_3 \xrightarrow{(-\ LiCl)} [P_2Cp]ZrCl_2(CH_2EMe_3)\ (\mathbf{7a}:\ E = C;\ \mathbf{7b}:\ E = Si) \quad (3)$$

The monoalkyl complexes **7a** and **7b** are each obtained as

$$[P_2Cp]ZrCl_3\ (\mathbf{1}) + 3\ LiCH_2EMe_3 \xrightarrow{(-\ 3\ LiCl)} [P_2Cp]Zr(CH_2EMe_3)_3\ (\mathbf{8a}:\ E = C;\ \mathbf{8b}:\ E = Si) \quad (4)$$

yellow oils that could not be isolated free of impurities. Some of the impurities arise from the slow disproportionation of **7** to give **1** and other unidentified species. Both **7a** and **7b** exhibit fluxional behavior similar to that observed for monobenzyl **2**,[26] although the processes could not be satisfactorily studied by variable-temperature NMR spectroscopy due to the inherent impurities.

The trialkyl complexes **8a** and **8b** can each be isolated cleanly as hydrocarbon-soluble oils. Singlets are observed in the ^{31}P NMR spectrum at −5.5 and −5.9 ppm for **8a** and **8b**, respectively. These resonances remain unchanged at lower temperatures and are indicative of dangling phosphines, as is found for tribenzyl **4**. Apparently, the crowded geometry imposed by three relatively bulky alkyl ligands prevents the phosphines from coordinating to the metal center.

Table 4. Rate Constants for the First-Order Portion of the Decomposition of **9b**

T (K)	$10^5 k_2$ (s^{-1})
353(1)	3.7(3)
368(1)	4.8(3)
383(1)	7.7(4)
398(1)	9.7(5)

A reexamination of the products obtained from the reaction of **1** with 2 equiv of $LiCH_2EMe_3$ reveals the presence of **7** and **8**, and another species which is observed as a singlet in the ^{31}P NMR spectrum and identified from the ^1H NMR spectrum as the dialkyl complex $[P_2Cp]ZrCl(CH_2EMe_3)_2$ (**9a:** E = C, **9b:** E = Si). Again, it seems that a similar equilibrium (eq 5) is established between **7**, **8**, and **9** for the neopentyl and neosilyl derivatives as has been observed for the benzyl derivative, since combining separate solutions of **7** and **8** produces the same mixture of all three species.

$$[P_2Cp]ZrCl_2(CH_2EMe_3)\ (\mathbf{7a}:\ E = C;\ \mathbf{7b}:\ E = Si) + [P_2Cp]Zr(CH_2EMe_3)_3\ (\mathbf{8a}:\ E = C;\ \mathbf{8b}:\ E = Si) \underset{K}{\rightleftharpoons} [P_2Cp]ZrCl(CH_2EMe_3)_2\ (\mathbf{9a}:\ E = C;\ \mathbf{9b}:\ E = Si) \quad (5)$$

Detailed analyses of these equilibria were precluded by the overlap of peaks in the ^1H and $^{31}P\{^1H\}$ NMR spectra for various species at separate temperatures. However, it could be ascertained that below the temperature at which one observes alkylidene formation, the equilibrium increasingly favors the disproportionation of the dialkyl species **9** as the temperature is raised (i.e., the value of *K* decreases with an increase in temperature), in contrast to the observations for **3** in the equilibrium of eq 2.

It is evident that the mechanistic details for the formation of the neopentyl and neosilyl alkylidene complexes **6** are similar to those previously outlined for benzylidene **5**. For example, heating either the monoalkyl **7** or trialkyl **8** derivatives independently does not generate an alkylidene complex, and the production of alkylidene from the thermolysis of the equilibrium mixture in eq 5 ceases when the supply of dialkyl precursor **9** has been exhausted. Once again this points to a mechanism analogous to that in Scheme 3, where the dialkyl complex **9** is the thermally labile species that leads directly to the alkylidene product in a first-order mechanism.

Experimental complications associated with the long reaction time and the formation of interfering impurities precluded a kinetic study of the neopentyl system. However, an analysis of the reaction kinetics for the thermal rearrangement of neosilyl **9b** was conducted by ^{31}P NMR spectroscopy, for reactions performed at 80, 95, 110, and 125 °C. In all instances the same pattern for the decrease in [**9b**] over time was observed as has been noted for benzyl **3** in Figure 1. Therefore, the results for **9b** were simulated by the same iterative procedure followed for **3**, from which the first-order rate constant (k_2) was obtained for each temperature (Table 4). The corresponding Eyring plot is shown in Figure 4, from which the activation parameters $\Delta H^{\ddagger} = 6(1)$ kcal mol^{-1} and $\Delta S^{\ddagger} = -62(5)$ cal mol^{-1} K^{-1} were

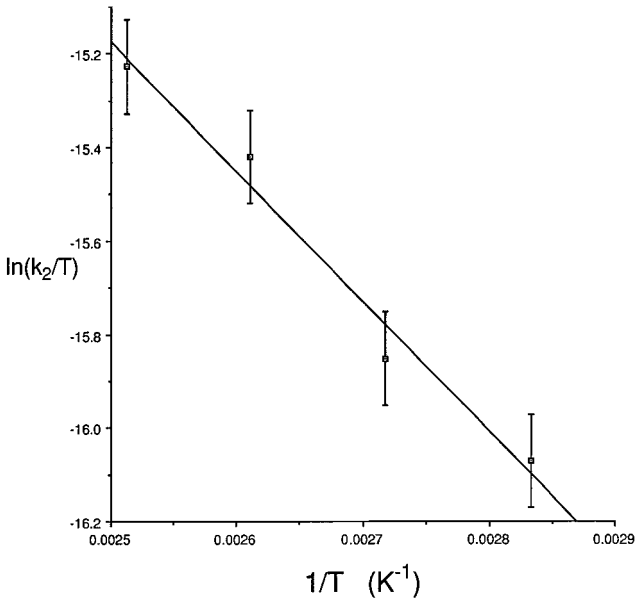

Figure 4. Eyring plot of the first-order decomposition of **9b** (arbitrary error bars of ±0.1 are indicated).

obtained; these values are significantly different from the parameters obtained for **3**.

The trend reported in the literature for the relative rates of alkylidene complex formation follows the order neopentyl > neosilyl > benzyl, which reflects faster rate-determining α-abstraction for complexes bound by alkyl ligands that can provide greater steric congestion at the metal center. For example, for the first-order decomposition of $Ta(CH_2R)_5$ (R = Ph, $SiMe_3$, CMe_3), the rate constants follow the order $k = 4.3 \times 10^{-5}$ (at 313 K) < 3.5×10^{-4} (311 K) < too fast to monitor, for R = Ph,[33] $SiMe_3$,[25] and CMe_3,[25] respectively. Our results indicate a *reversal* of this trend for the complexes studied here. The neopentyl system that produces alkylidene **6a** was found to be too slow to study, and a comparison of the first-order rate constants in Table 2 and Table 4 for the dialkyl species studied reveals the slower thermal reactivity of neosilyl **9b** versus benzyl **3**. This surprising observation may be partially related to the unusual preequilibrium step associated with the postulated mechanism (Scheme 3), where disproportionation of the dialkyl species is favored at higher temperatures for the bulkier derivatives, in competition with the irreversible step leading to alkylidene formation. However, the effect of the preequilibrium is evidently secondary in comparison to the activation parameters, particularly $\Delta S^{\ddagger}$, associated with the rate-determining α-abstraction step. As mentioned above, both near-zero and negative values (0 to −10 cal mol^{-1} K^{-1}) have been typically observed for the majority of C−H bond abstraction processes that have been studied. The results from this work show considerable departure from these values, especially with the large negative $\Delta S^{\ddagger}$ of −62(5) cal mol^{-1} K^{-1} for **9b**, which has been rarely seen for a first-order process. To account for this remarkable difference it is useful to examine the proposed transition state structure in this reaction as shown in Scheme 5. For the dibenzyl complex **3**, the $^{31}P\{^1H\}$ NMR data indicate that one phosphine binds in the ground state; to access the transition state, there are two features that must be attained, both of which lead to a significantly more ordered structure in the transition state in comparison to the ground state structure of the dialkyl derivatives, which could generate a relatively large negative $\Delta S^{\ddagger}$ term. The first is the coordination of both bulky sidearm phosphines, considered to help lower the activation energy by increasing steric saturation at the metal center to induce α-abstraction as a means of relieving the steric pressure. The second feature is the necessity for the two alkyl ligands to attain a cis configuration to permit the concerted abstraction step to proceed via the four-centered transition state. The steric difficulties that must be surmounted to reach the transition state are even more pronounced for the bulkier dialkyl species **9b**. For example, the singlet in the $^{31}P\{^1H\}$ NMR spectrum for **9b** at −4.5 ppm is consistent with uncoordinated phosphine donors as shown in Scheme 5. In this case, the difference between the ground state, in which both arms are unbound, and the highly ordered transition state leads to the very large negative $\Delta S^{\ddagger}$. Since the $\Delta H^{\ddagger}$ terms for these processes do not differ much from $Ta(CH_2R)_5$ systems discussed above, it is the large negative value of $\Delta S^{\ddagger}$ for the bulkier alkyl derivatives that results in the observed reversal of the reactivity trend; in other words, entropic factors are important in the formation of these group 4 alkylidene complexes. These factors also help to explain the otherwise contradictory observation that the bulky trialkyl derivatives are thermally unreactive, as these complexes are too sterically hindered in comparison to the dialkyl analogues to allow the bulky phosphines to coordinate in the transition state.

Scheme 5

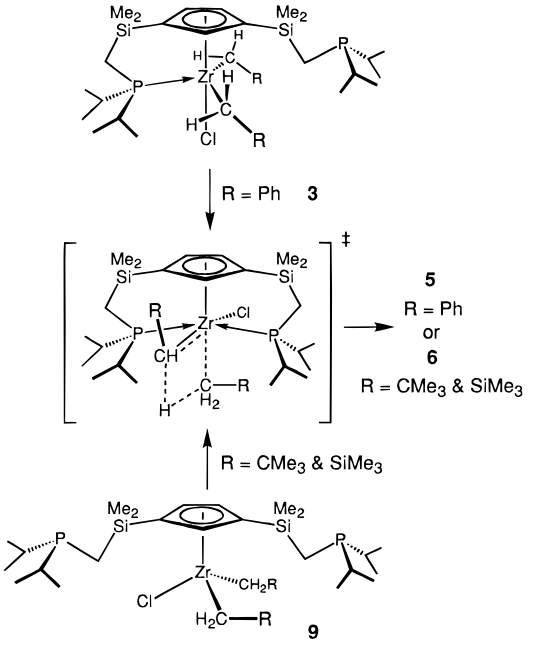

Conclusions

The ancillary ligand [P_2Cp] has been utilized in the synthesis of the first reported examples of stable zirconium alkylidene complexes, **5** and **6b**. The structural parameters are similar for each and the solid-state structure is maintained in solution. Both complexes are monomeric with C_s symmetry, and the alkylidene units are oriented in a similar fashion with respect to the ancillary ligand. An agostic interaction between the alkylidene α-C−H moiety and the metal center is also present in both compounds, a common feature for unsaturated alkylidene complexes.

The alkylidene complexes **5** and **6** are formed via the thermal decomposition of the corresponding dialkyl precursors **3** and **9**, respectively. However, this is complicated by a preequilibrium step in which **3** and **9** also undergo reversible ligand redistribution, presumably via a bridging dinuclear adduct, to give the

(33) Malatesta, V.; Ingold, K. U.; Schrock, R. R. *J. Organomet. Chem.* **1978**, *152*, C53.

corresponding mono and tris(alkyl) species (Scheme 2). Kinetic studies show that the decomposition of **3** and **9** follows first-order kinetics, with a deviation in the first-order plot associated with the presence of the preequilibrium. The activation parameters obtained from the reaction are consistent with an intramolecular α-abstraction process, as is the kinetic isotope effect of 3.0 (0.5) obtained for the benzyl derivative. However, in the systems studied here the reaction rates follow the order benzyl > neosilyl > neopentyl, exactly opposite to that found previously in other systems. These results reflect a subtle balance between the steric crowding imposed by the alkyl ligands and the sidearm phosphines of the ancillary ligand. The bulkier neopentyl ligands crowd the metal center to a greater extent than do the benzyl groups, thus providing less opportunity for the relatively large Pr^i_2P donors to coordinate. As alkylidene formation can be promoted by phosphine coordination,[34] this may account for the faster rates observed for the less bulky benzyl derivative, in addition to the otherwise surprising lack of thermal reactivity of the trialkyl species, where phosphine coordination remains absent under all conditions.

Experimental Section

General Considerations. All manipulations were performed under an atmosphere of prepurified nitrogen in a Vacuum Atmospheres HE-553-2 glovebox equipped with a MO-40-2H purification system or in standard Schlenk-type glassware on a dual vacuum/nitrogen line. ^{1}H NMR spectra (referenced to nondeuterated impurity in the solvent) were performed on one of the following instruments depending on the complexity of the particular spectrum: Bruker WH-200, Varian XL-300, or a Bruker AM-500. ^{13}C NMR spectra (referenced to solvent peaks) were run at 75.429 MHz on the XL-300 instrument, and ^{31}P NMR spectra (referenced to external $P(OMe)_3$ at 141.0 ppm) were run at 121.421 and 202.33 MHz on the XL-300 and Bruker AM-500 instruments, respectively. All chemical shifts are reported in ppm and all coupling constants are reported in Hz. Elemental analyses were performed by Mr. P. Borda of this department.

Reagents. Hexanes and tetrahydrofuran (THF) were predried over CaH_2 followed by distillation from sodium-benzophenone ketyl under argon. Toluene was dried over sodium under argon, and hexamethyldisiloxane was distilled from sodium-benzophenone ketyl under nitrogen. The deuterated solvents C_6D_6 and $C_6D_5CD_3$ were dried over molten sodium, vacuum transferred to a bomb, and degassed by freeze−pump−thaw technique before use. KCH_2Ph (and the perdeuterated analogue $KCD_2C_6D_5$), $LiCH_2CMe_3$, and $LiCH_2SiMe_3$ were prepared according to literature methods. $(\eta^5\text{-}C_5H_5)_2Fe$ (ferrocene) was sublimed before use, and trimethylphosphine was vacuum distilled by vacuum transfer. Samples of ferrocene and PMe_3 were dissolved in benzene-d_6 and prepared in sealed melting point tubes for ^{1}H NMR external reference. The procedures for the preparation of $[P_2Cp]ZrCl_3$ (**1**),[26] $[P_2Cp]ZrCl_2(CH_2Ph)$ (**2**),[26] $[P_2Cp]Zr(CH_2Ph)_3$ (**4**),[26] and $[P_2Cp]Zr{=}CHPh(Cl)$ (**5**)[24] have been described elsewhere.

$[P_2Cp]ZrCl(CH_2Ph)_2$ (3). (a) From $[P_2Cp]ZrCl_3$ (1) and KCH_2Ph. A solution of KCH_2Ph (0.100 mg, 0.43 mmol) in 10 mL of THF was added with stirring to a cooled (−78 °C) solution of **1** (65 mg, 0.23 mmol) dissolved in 30 mL of THF. The dark red color of the KCH_2Ph solution was discharged upon addition and the color of the reaction mixture became greenish-orange. The mixture was allowed to slowly warm to room temperature, whereupon all the volatiles were then removed under vacuum and the residue extracted with hexanes and filtered. The filtrate was reduced under vacuum to give a thermally and photochemically labile sensitive orange oil. NMR spectra of this oil indicate the presence of **3**, in addition to both **2** and **4**.

(b) From $[P_2Cp]ZrCl_2(CH_2Ph)$ (2) and $[P_2Cp]Zr(CH_2Ph)_3$ (4). Mixing together stoichiometric benzene-d_6 solutions of **2** and **4** produced a mixed solution with the same spectroscopic results as observed for procedure (a) above.

(34) Rupprecht, G. A.; Messerle, L. W.; Fellmann, J. D.; Schrock, R. R. *J. Am. Chem. Soc.* **1980**, *102*, 6236.

The assignment of resonances for **3** is based on the known resonances for **2** and **4**. Note that some peaks for **3** are obscured by overlapping resonances arising from **2** and **4**.

3: ^{1}H NMR (20 °C, C_6D_6) δ 0.33 and 0.44 (s, 6H, $Si(CH_3)_2$), 0.89 (m, 4H, $SiCH_2P$), 1.23 (m, 24H, $CH(CH_3)_2$), 2.34 (m, 4H, CH_2Ph), 6.49 (d, 2H, $^4J_{HH}$ = 1 Hz, Cp-*H*), 6.65 (d, 4H, $^4J_{HH}$ = 7 Hz, *o*-C_6H_5), 6.87 (t, 1H, $^4J_{HH}$ = 1 Hz, Cp-*H*), 7.03 (t, 4H, $^3J_{HH}$ = 7 Hz, *m*-C_6H_5), 7.22 (t, 2H, $^3J_{HH}$ = 7 Hz, *p*-C_6H_5). ^{31}P{^{1}H} NMR (20 °C, C_6D_6) δ 0.1 (s).

$[P_2Cp]ZrCl_2(CH_2CMe_3)$ (7a). A solution of $LiCH_2CMe_3$ (19 mg, 0.24 mmol) in 30 mL of toluene was added dropwise over a period of 20 min to a cooled (−78 °C) stirring solution of **1** (156 mg, 0.24 mmol) dissolved in 60 mL of toluene. The color of the solution gradually changed from pale to bright yellow. The solution was stirred at −78 to 0 °C for another 30 min, and then allowed to warm slowly to room temperature. The solvent was then removed in vacuo, and the oily residue extracted with hexanes and filtered. The filtrate was reduced to yield 0.87 g of a slightly impure (by ^{1}H and ^{31}P NMR spectroscopy) yellow oil consisting of **6a** as the main (>90%) product. ^{1}H NMR (20 °C, C_6D_6) δ 0.26 and 0.36 (s, 6H, $Si(CH_3)_2$), 0.70 (dd, 4H, $^2J_{HH}$ = 6 Hz, $^2J_{PH}$ = 7 Hz, $SiCH_2P$), 1.00 (m, 24H, $CH(CH_3)_2$), 1.47 (s, 9H, $CH_2C(CH_3)_3$), 1.52 (m, 4H, $CH(CH_3)_2$), 1.68 (s, 2H, $CH_2C(CH_3)_3$), 6.54 (t, 1H, $^4J_{HH}$ = 1 Hz, Cp-*H*), 6.98 (d, 2H, $^4J_{HH}$ = 1 Hz, Cp-*H*). ^{31}P NMR (20 °C, C_6D_6) δ 0.7 (br s).

$[P_2Cp]ZrCl_2(CH_2SiMe_3)$ (7b). The procedure followed was similar to that for **6a**, using $LiCH_2SiMe_3$ (27 mg, 0.29 mmol) and **1** (185 mg, 0.29 mmol), to yield an impure yellow oil (>85% pure by ^{1}H and ^{31}P NMR spectroscopy). ^{1}H NMR (20 °C, C_6D_6) δ 0.31 (s, 9H, $CH_2Si(CH_3)_3$), 0.38 and 0.50 (s, 6H, $Si(CH_3)_2$), 0.69 (s, 2H, $CH_2Si(CH_3)_3$), 0.71 (dd, 4H, $^2J_{HH}$ = 6 Hz, $^2J_{PH}$ = 7 Hz, $SiCH_2P$), 1.05 (m, 24H, $CH(CH_3)_2$), 1.61 (m, 4H, $CH(CH_3)_2$), 6.50 (t, 1H, $^4J_{HH}$ = 1 Hz, Cp-*H*), 7.05 (d, 2H, $^4J_{HH}$ = 1 Hz, Cp-*H*). ^{31}P NMR (20 °C, C_6D_6) δ 1.5 (br s).

$[P_2Cp]ZrCl(CH_2CMe_3)_2$ (9a). A solution of $LiCH_2CMe_3$ (1.09 mg, 0.24 mmol) in 60 mL of toluene was added dropwise to a cooled (−78 °C) stirring solution of **1** (350 mg, 0.58 mmol) dissolved in 60 mL of toluene. The color of the solution immediately changed in intensity from pale to bright yellow. The solution was allowed to warm slowly to room temperature and stirred for another 2 h. The solvent was then removed in vacuo, and the residue extracted with hexanes and filtered. The filtrate was reduced to give a bright yellow oil consisting of **7a,** in addition to **6a** and **8a**. The assignment of resonances for **7a** is based on the known resonances for **6a** and **8a** obtained by independent syntheses. ^{1}H NMR (20 °C, C_6D_6) δ 0.45 and 0.47 (s, 6H, $Si(CH_3)_2$), 0.63 (d, 4H, $^2J_{HH}$ = 6 Hz, $SiCH_2P$), 0.89 (m, 24H, $CH(CH_3)_2$), 1.23 (s, 18H, $CH_2C(CH_3)_3$), 1.31 and 1.78 (d, 2H, $^2J_{HH}$ = 8 Hz, $CH_2C(CH_3)_3$), 1.55 (m, 4H, $CH(CH_3)_2$), 6.82 (d, 2H, $^4J_{HH}$ = 1 Hz, Cp-*H*), 7.03 (t, 1H, $^4J_{HH}$ = 1 Hz, Cp-*H*). ^{31}P NMR (20 °C, C_6D_6) δ −5.9 (s).

$[P_2Cp]ZrCl(CH_2SiMe_3)_2$ (9b). The procedure followed is analogous to that for **9a** above, using $LiCH_2SiMe_3$ (117 mg, 1.24 mmol) and **1** (398 mg, 0.62 mmol). The resulting greenish oil consists of **7b**, **8b**, and **9b**. Again, the assignment for **9b** is based on integration of the ^{1}H NMR spectrum. ^{1}H NMR (20 °C, C_6D_6) δ 0.32 (s, 18H, $CH_2Si(CH_3)_3$), 0.41 and 0.43 (s, 6H, $Si(CH_3)_2$), 0.63 (d, 4H, $^2J_{HH}$ = 6 Hz, $SiCH_2P$), 0.70 and 1.14 (d, 2H, $^2J_{HH}$ = 12 Hz, $CH_2Si(CH_3)_3$), 0.99 (m, 24H, $CH(CH_3)_2$), 1.57 (m, 4H, $CH(CH_3)_2$), 6.81 (t, 1H, $^4J_{HH}$ = 1 Hz, Cp-*H*), 6.86 (d, 2H, $^4J_{HH}$ = 1 Hz, Cp-*H*). ^{31}P NMR (20 °C, C_6D_6) δ −4.5 (s).

$[P_2Cp]Zr(CH_2CMe_3)_3$ (8a). A solution of $LiCH_2CMe_3$ (56 mg, 0.72 mmol) in 30 mL of toluene was added dropwise to a cooled (−78 °C) stirring solution of **1** (154 mg, 0.24 mmol) dissolved in 60 mL of toluene. The color of the solution immediately turned bright yellow upon addition. The mixture was warmed to room temperature, and stirring was continued for 30 min. The solvent was then removed in vacuo, and the oily residue extracted with hexanes and filtered. The filtrate was reduced under vacuum to give **8a** as a bright yellow oil that remained soluble in pentane even at −40 °C, precluding the isolation of crystalline material. Yield 130 mg, 72%. ^{1}H NMR (20 °C, C_6D_6) δ 0.48 and 0.49 (s, 6H, $Si(CH_3)_2$), 0.70 (dd, 4H, $^2J_{HH}$ = 6 Hz, $^2J_{PH}$ = 4 Hz, $SiCH_2P$), 0.99 (m, 24H, $CH(CH_3)_2$), 1.21 (s, 6H, $CH_2C(CH_3)_3$), 1.22 (s, 27H, $CH_2C(CH_3)_3$), 1.55 (m, 4H, $CH(CH_3)_2$), 6.68 (d, 2H, $^4J_{HH}$ = 1 Hz, Cp-*H*), 6.94 (t, 1 Hz, $^4J_{HH}$ = 1H, Cp-*H*). ^{31}P NMR (20 °C, C_6D_6) δ −5.5 (s).

Table 5. Crystallographic Data[a]

compound	**6b**[a]	transmission factors	0.823−0.999
formula	$C_{27}H_{57}ClP_2Si_2Zr$	scan type	$\omega-2\theta$
fw	654.62	data collected	$\pm h,+k,+l$
crystal system	monoclinic	$2\theta_{max}$, deg	45
space group	$P2_1/n$ (No. 14)	total reflcns	4817
a, Å	12.982(5)	unique reflcns	4640
b, Å	16.679(6)	R_{merge}	0.040
c, Å	16.710(5)	no. with $I \geq 3\sigma(I)$	3028
α, deg	76.50(3)	no. of variables	311
β, deg	90	$R(F)$ ($I \geq 3\sigma(I)$)	0.056
γ, deg	90	$R_w(F)$ ($I \geq 3\sigma(I)$)	0.055
V, Å^3	3573(22)	$R(F^2)$ (all data)	0.056
Z	4	$R_w(F^2)$ (all data)	0.055
D_{calc}, g/cm^3	1.22	gof	3.16
F(000)	1392	max Δ/σ (final cycle)	0.000
μ, cm^{-1}	5.1	residual density e/Å^3	−0.610 to 0.880 (near Zr)
crystal size, mm	0.30 × 0.40 × 0.50		

[a] Temperature 294 K, Nonius CAD-4 diffractometer, Mo $K\alpha$ radiation ($\lambda = 0.70930$ Å), graphite monochromator, takeoff angle 6.0°, aperture 6.0 × 6.0 mm at a distance of 285 mm from the crystal, stationary background counts at each end of the scan (scan/background time ratio 2:1), $\sigma^2(F^2) = [S^2(C + 4B)]/Lp^2$ (S = scan rate, C = scan count, B = normalized background count), function minimized $\sum w(|F_o| - |F_c|)^2$ where $w = 4F_o^2/\sigma^2(F_o^2)$, $R(F) = \sum||F_o| - |F_c||/\sum|F_o|$, $R_w(F) = (\sum w(|F_o| - |F_c|)^2/\sum w|F_o|^2)^{1/2}$, and gof ($F$) $= [\sum w(|F_o| - |F_c|)^2/(m - n)]^{1/2}$.

[P$_2$Cp]Zr(CH$_2$SiMe$_3$)$_3$ (8b). The procedure followed was similar to that for **8a**, using $LiCH_2SiMe_3$ (82 mg, 0.87 mmol) and **1** (185 mg, 0.29 mmol), to yield a pale yellow oil. Yield 176 mg, 76%. ^{1}H NMR (20 °C, C_6D_6) δ 0.28 (s, 27H, $CH_2Si(CH_3)_3$), 0.29 and 0.45 (s, 6H, $Si(CH_3)_2$), 0.32 and 0.63 (d, 2H, $^2J_{HH} = 6$ Hz, $SiCH_2P$), 0.68 (s, 6H, $CH_2Si(CH_3)_3$), 1.00 (m, 24H, $CH(CH_3)_2$), 1.59 (m, 4H, $CH(CH_3)_2$), 6.74 (d, 2H, $^4J_{HH} = 2$ Hz, Cp-*H*), 6.91 (t, 1H, $^4J_{HH} = 2$ Hz, Cp*H*). ^{31}P NMR (20 °C, C_6D_6) δ −5.9 (s).

[P$_2$Cp]Zr=CHCMe$_3$(Cl) (6a). A solution of $LiCH_2CMe_3$ (51 mg, 0.65 mmol) in 20 mL of toluene was added dropwise with stirring to a cooled (−78 °C) solution of **1** (210 mg, 0.33 mmol) dissolved in 60 mL of toluene. The color of the solution immediately changed to bright yellow. The solution was stirred at −78 to 0 °C for another 30 min, and then for another 3 h at room temperature. The solvent was then removed in vacuo, and the residue extracted with hexanes and filtered. The filtrate was reduced under vacuum to give a green oil that was redissolved in 30 mL of toluene. This solution was placed in a 95 °C oil bath for 6 days, after which no further reaction could be detected by NMR spectroscopy. The solvent was removed, and the oil extracted with pentane to give a green oil, containing **6a** and other unidentified products. Repeated attempts to obtain crystals from cold pentane were unsuccessful. Estimated yield 65% by ^{31}P NMR spectroscopy. ^{1}H NMR (20 °C, C_6D_6) δ 0.38 and 0.40 (s, 6H, $Si(CH_3)_2$), 0.80 (dd, 4H, $^2J_{HH} = 6$ Hz, $^2J_{PH} = 7$ Hz, $SiCH_2P$), 1.10 and 1.30 (m, 12H, $CH(CH_3)_2$), 1.50 (s, 9H, $CHC(CH_3)_3$), 2.10 (m, 4H, $CH(CH_3)_2$), 6.60 (d, 2H, $^4J_{HH} = 1$ Hz, C_5H), 7.41 (t, 1H, $^4J_{HH} = 1$ Hz, C_5H), 8.20 (s, 1H, $CHC(CH_3)_3$). ^{31}P NMR (20 °C, C_6D_6) δ 14.0 (s).

[P$_2$Cp]Zr=CHSiMe$_3$(Cl) (6b). A solution of $LiCH_2SiMe_3$ (155 mg, 1.64 mmol) in 30 mL of toluene was added dropwise with stirring to a cooled (−78 °C) solution of **1** (525 mg, 0.82 mmol) dissolved in 90 mL of toluene. The color of the solution immediately changed from pale yellow to bright yellowish green. The solution was stirred at −78 to 0 °C for another 30 min, and then for another 2 h at room temperature. The solvent was then removed, and the residue extracted with hexanes and filtered. The filtrate was reduced under vacuum to give a greenish yellow oil that was redissolved in 60 mL of toluene. This solution was placed in a 95 °C oil bath for 3 days, after which the volume was reduced under vacuum to 1 mL and 5 mL of hexanes added. Bright yellow crystals were slowly obtained from this concentrated solution at −40 °C. The supernatant solution was filtered away, and the crystals washed twice with cold hexanes and dried under vacuum. More crystalline material could be obtained from the mother liquor. Yield 440 mg, 82%. ^{1}H NMR (20 °C, C_6D_6) δ 0.21 and 0.53 (s, 6H, $Si(CH_3)_2$), 0.32 (s, 9H, $CHSi(CH_3)_3$), 0.68 and 0.72 (dd, 4H, $^2J_{HH} = 6$ Hz, $^2J_{PH} = 7$ Hz, $SiCH_2P$), 1.04 and 1.48 (m, 12H, $CH(CH_3)_2$), 2.11 and 2.29 (m, 2H, $CH(CH_3)_2$), 6.07 (d, 2H, $^4J_{HH} = 1$ Hz, C_5H), 7.30 (t, 1H, $^4J_{HH} = 1$ Hz, C_5H), 8.99 (s, $CHSi(CH_3)_3$). ^{31}P NMR (20 °C, C_6D_6) δ 16.2 (s). ^{13}C NMR (20 °C, C_6D_6) δ 5.9 and 11.1 ($Si(CH_3)_2$), 7.9 ($CH(CH_3)_2$), 16.5 ($SiCH_2P$), 25.6 and 30.9 ($CH(CH_3)_2$), 26.6 ($CHSi(CH_3)_3$), 35.4 and 35.5 ($CH(CH_3)_2$), 119.0 (Cp-CH2), 121.9 (CpSi), 129.5 (Cp-CH), 213.8 (t, $^2J_{CP} = 12$ Hz, $CHSi(CH_3)_3$). Anal. Calcd for $C_{27}H_{57}ClP_2Si_3Zr$: C, 49.54; H, 8.78; Cl, 5.42. Found: C, 49.58; H, 8.71; Cl, 5.65.

NMR Study of the Equilibrium between 2, 3, and 4. Separate stock solutions of **2** and **4** were prepared in benzene-d_6, the concentrations of which were determined by comparing the integrated intensity of the CH_2Ph signals relative to external ferrocene. Incrementally varied proportions of the initial solutions of **2** and **4** were then combined together to generate mixed solutions consisting of **2**, **3**, and **4**. ^{1}H NMR spectra of these solutions were obtained, and the concentrations of **2**, **3**, and **4** were calculated from the integration of the CH_2Ph signals with respect to that of the ferrocene standard.

Kinetic Studies of the Formation of Alkylidene 5 and 6b. A sample of the equilibrium mixture consisting of monobenzyl **2**, dibenzyl **3**, and tribenzyl **4** was dissolved in toluene-d_8 and used as a stock solution for kinetic study. The initial concentrations in this solution were calculated from the integration of the ^{31}P NMR signals of a representative sample with respect to that of the internal standard PPh_3. The disappearance of **3** and **4** (and the concomitant appearance of **5**) as recorded by ^{31}P{^{1}H} NMR spectroscopy was monitored for a period of at least 3 half-lives; samples with an internal PPh_3 reference were employed to calibrate the measurements. Separate kinetic runs were conducted on the Varian 300-XL instrument at temperatures set to 70, 80, 85, and 90 °C. The uncertainty in the temperature settings was estimated to be ±1 °C. Similar experiments with the $CD_2C_6D_5$ labeled complexes were performed at 70 °C to examine kinetic isotope effects (KIE) associated with the proposed mechanism. Each experiment was repeated at least once to indicate reproducibility. For the duration of the kinetic experiments, all sample tubes were protected from light sources where possible by using metal foil wrap to minimize the competitive photochemical transformation of **3** to **5**.

A similar procedure was followed for the study into the formation of the silyl alkylidene **6b**, except the ^{31}P{^{1}H} NMR spectra were conducted at 20 °C, as the resonances due to dialkyl **9b** and trialkyl **8b** merge together at higher temperatures. For a typical run, a 0.5 mL sample of the toluene solution was placed in a 5 mm NMR tube, the solution frozen and degassed, and the tube then flame sealed and placed in a constant temperature oil bath (uncertainty in the temperature measurements estimated to be 1 °C). The tube was removed from the bath after a period of 1.5 h and immersed in an ice bath to quench the reaction. A ^{31}P{^{1}H} NMR spectrum was recorded at 20 °C on the Bruker-AMX 500 MHz instrument, and the tube returned to the oil bath. This procedure was repeated with further 1.5 h heating intervals, and the disappearance of **9b** and **8b** (and the concomitant appearance of **6b**) as recorded by ^{31}P{^{1}H} NMR spectroscopy was monitored for a period of at least 3 half-lives. Kinetic experiments were conducted at four different temperatures (80, 95, 110, and 125 °C) to obtain separate reaction rates.

X-ray Data Collection and Reduction. X-ray quality crystals of **6b** were obtained from the preparation as described above. A representative crystal was mounted and sealed within a capillary to maintain a dry, O_2-free environment for the sample during the crystallographic analysis. Diffraction experiments were performed at 23 °C on a Nonius CAD-4 diffractometer equipped with graphite-monochromatized Mo Kα (0.70930 Å) radiation. The final unit-cell parameters were obtained by least-squares for 24 reflections with $2\theta = 30.00-43.00$ degrees. The data were processed and corrected for Lorentz and polarization effects, and absorption.

The structure was solved by conventional heavy atom methods, the coordinates of the Zr, P, and Si atoms being determined from the Patterson function and those of the remaining atoms from subsequent difference Fourier syntheses. After anisotropic refinement of all non-hydrogen atoms, methylene and ring sp^2 hydrogen atoms were fixed in calculated positions ($d_{C-H} = 1.08$ Å) with temperature factors based upon the carbon to which they are bonded. Methyl hydrogen atoms were located and fixed via inspection of a difference Fourier map, temperature factors based upon the carbon to which they are bonded. H19 was located via difference Fourier map inspection and refined. All crystallographic calculations were conducted with the PC version of the NRCVAX program package locally implemented on an IBM-compatible 80486 computer.

Crystallographic data appear in Table 5.

Acknowledgment. Financial support for this research was provided by NSERC of Canada in the form of a Research Grant to M.D.F. and a postgraduate scholarship to P.B.D.

Supporting Information Available: Additional tables include crystallographic data and atomic positional and thermal parameters for **6b** (PDF). This material is available free of charge via the Internet at http://pubs.acs.org.

JA982969H